Foucault's method for measuring the speed of light with modern apparatus

2015 Eur. J. Phys. 36 035013

(http://iopscience.iop.org/0143-0807/36/3/035013)

IOP Publishing European Journal of Physics
Eur. J. Phys. **36** (2015) 035013 (14pp) doi:10.1088/0143-0807/36/3/035013

Foucault's method for measuring the speed of light with modern apparatus

Zoltán Vörös[1] **and Gregor Weihs**

Institut für Experimentalphysik, Universität Innsbruck, Technikerstraße 25, Innsbruck, A-6020, Austria

E-mail: zvoros@uibk.ac.at

Received 19 January 2015
Accepted for publication 13 February 2015
Published 19 March 2015

Abstract

In this paper, we introduce two simple and inexpensive, yet quite accurate versions of the well-known Foucault method for measuring the speed of light. In a compact footprint of just 20 cm by 270 cm with readily available laboratory items, a rotating mirror taken from a laser printer, and a webcam, we obtained $c = 296\,720 \pm 3000\ \mathrm{km\,s^{-1}}$, and $c = 302\,295 \pm 3000\ \mathrm{km\,s^{-1}}$, respectively, both within less than a per cent of the defined value. The experiment also prepares students for extracting data through image processing.

Keywords: speed of light, experiment, optics, data processing

1. Introduction

As has been well known since 1983 [1], we cannot actually measure the vacuum speed of light, but merely calibrate our metre stick using the defined value of $299\,792\,458\ \mathrm{m\,s^{-1}}$. Nevertheless, we find that Foucault's method has great elegance and pedagogical value in that it uses relatively simple means like a mirror spinning at very reasonable frequencies to derive a measurable shift from the large but finite value of the speed of light.

While Foucault's method is a staple in many elementary physics lab courses and the hardware for it is sold by various suppliers [2, 3] it also traditionally yields only relatively poor precision and accuracy. The limited precision is linked to taking data using a microscope ruler, whereas the poor accuracy stems mostly from difficulties in determining the various distances in the experiment. We have developed a new version of Foucault's method that improves both precision and accuracy while employing very inexpensive and even in part recycled components. It also introduces students to taking data using imaging devices and image processing.

[1] Author to whom any correspondence should be addressed.

The paper is organized as follows. In the next two sections, we outline the historical and theoretical background and derive the expression for c. In section 4, we introduce our experimental setup and the critical components, section 5 contains a detailed discussion of our results, while section 6 is devoted to a thorough analysis of various systematic errors. In the appendix, we present a couple of MATLAB (The Mathworks, Inc.) snippets that can be used to evaluate measurement data.

2. Historical background

That the speed of light, c, is finite was already conjectured by Galileo in the 17th century, though his experimental apparatus at the time prevented him from giving even an order-of-magnitude estimate for the value. Since then, various methods have been developed.

It was first Huygens, who, based on the astronomical measurements of Rømer in 1676 on the entry into and exit from eclipses of Jupiter's moons, could provide a lower bound of about $200\,000\,\mathrm{km\,s^{-1}}$. The same measurements, repeated with higher accuracy by Delambre in 1809, yielded $304\,000\,\mathrm{km\,s^{-1}}$, astonishingly close to the true value. Another astronomical method, the aberration of light, was discovered by Bradley in 1729, with the result of about $296\,000\,\mathrm{km\,s^{-1}}$.

Later, it was realized that in Maxwell's theory, the speed of light is linked to fundamental electromagnetic constants through the relation $\epsilon_0\mu_0 = c^{-2}$, and therefore, by measuring the vacuum permittivity ϵ_0, and the vacuum permeability μ_0, it is possible to indirectly infer the value of c [4, 5].

It is also to be noted that, if the frequency f of electromagnetic radiation is known, and the wavelength λ can be measured, then by dint of the relation $c = f\lambda$, c can be indirectly determined. This is the basis of measurements of interferometric methods [6, 7], and of cavity resonance methods [8]. It is further the basis with which to derive the SI metre from the definition of c, and the SI second.

Finally, there are several methods that measure the time of flight in terrestrial settings. One of them is the Foucault method that we discuss in more detail in the next section [9–12], while with the advent of high-speed electronics, it is now possible to directly measure the delay in the arrival of short optical pulses as the distance between the emitter and receiver is increased [13–16]. This latter method is the simplest of all, but it definitely lacks the elegance of the others.

The interested reader can find a more detailed survey of various measurement methods and their significance in [17].

3. Theoretical background

Foucault's is one of the simplest methods of measuring the speed of light on Earth, and it falls into the category of time of flight measurements. It is based on the observation that, if a light beam bounces off a moving mirror twice, the mirror will have moved by a small amount by the time it is hit by the beam the second time, and this movement results in a small displacement of the reflected beam. It is this displacement that is to be measured, and from where the speed of light is to be inferred. In this particular instance, the mirror is rotating, and the rotation angle between the two events can simply be related to the time that was required for the round trip. The speed of light can be obtained from the measured displacement, and the length of the round-trip path. Due to its conceptual simplicity, this is perhaps the most popular method in student laboratories.

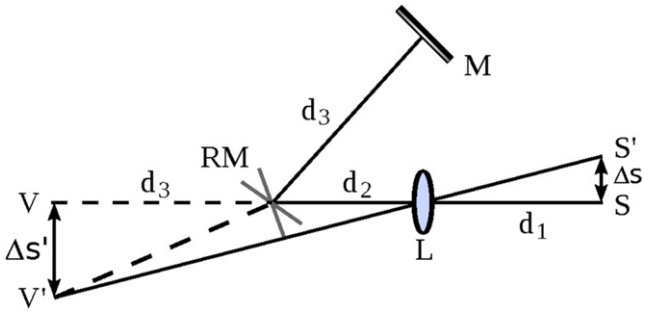

Figure 1. The concept of the experiment. RM is the rotating mirror, M is the end reflector, and L is a lens. S, S' are the light source, and its image, respectively, while V, and V' are the virtual images of S, and S'.

To be more specific, let us take the simplified experimental setup shown in figure 1. A point source emitting light is located at point S, at a distance d_1 from the lens L. The source's light is reflected by the rotating mirror (RM) (at a distance of d_2 from the lens, and at this point, stationary) and its image is created at the position of the end mirror M, which is at a distance of d_3 from the RM, and is normal to the in-coming light. This also means that the light reflected by M is focused on S again. In the absence of the RM, the image of S would be at V.

Now, let us assume that in the time Δt the light traverses the distance between RM and M in both directions, the RM turns by an amount $\omega\Delta t$, where ω is the angular velocity, and $\Delta t = 2d_3/c$. This rotation displaces the virtual image V to V', where the distance between these two points is simply $\Delta s' = 2\omega\Delta t \cdot d_3$. The factor of 2 is a result of the reflection on RM: upon reflection, all angles change by a factor of 2. The image of the virtual point V' is mapped by the lens to the point S', and using the two similar triangles formed by V, V', and the lens, and S, S', and the lens, respectively, we conclude that the distance between S and S' is

$$\Delta s = \frac{d_1}{d_2 + d_3}\Delta s' = 2\omega\Delta t\frac{d_1 d_3}{d_2 + d_3} = \frac{4d_1 d_3^2}{d_2 + d_3}\frac{\omega}{c},$$

i.e., the speed of light is

$$c = \frac{4d_1 d_3^2}{d_2 + d_3}\frac{\omega}{\Delta s}. \tag{1}$$

Given $d_{1,2,3}$, the speed of light can be gotten by measuring the displacement Δs for a given angular speed. In principle, to determine c, a single measurement point is enough, but as we will see later, by measuring Δs as a function of ω, and taking the slope of the linear dependence, it is not necessary to find the reference position at $\omega = 0$. Re-arranging equation (1) yields

$$c_0 = \frac{4d_1 d_3^2}{d_2 + d_3}\left(\frac{\mathrm{d}\Delta s}{\mathrm{d}\omega}\right)^{-1}. \tag{2}$$

In section 6, we will show that the errors are negligible, if the lens is not positioned perfectly, and the image of S is not formed at M. In the formula above, c_0 indicates that these errors are not yet taken into account.

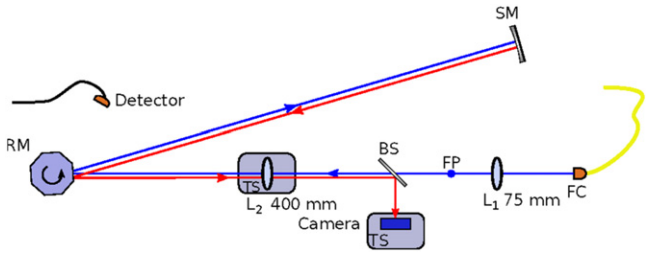

Figure 2. Experimental setup, setup 1. RM, FM, SM are the rotating, folding, and back reflector mirrors, respectively, L_1, L_2 are lenses of focal length 75 and 400 mm, respectively, FP is the focal point of L_1, FC is the fibre collimator, BS is the beamsplitter, and TS are translation stages. Dimensions are given in the text.

4. Experimental setup

Figure 2 displays our first experimental setup. Laser light from a standard fibre fault locator (OZ Optics, FODL-43S-635-1) emitting at a wavelength of 635 nm is transmitted through a single-mode fibre, and collimated by a short focal length fibre collimator (Thorlabs F240FC-B). While it is not absolutely necessary, by passing the light through the single-mode fibre patch cable (Thorlabs P1-630A-FC-1), we begin with a perfect Gaussian beam. It is worth noting that the fault locator can be replaced by an inexpensive laser pointer.

The collimated beam is then led through a telescope consisting of two lenses of focal lengths 75 (L_1), and 400 mm (L_2), respectively. The telescope is misaligned slightly in the longitudinal direction (the distance between the two lenses is larger than 475 mm), so that the beam leaving is not collimated any more, but, after being reflected on the RM, is focused on a spherical mirror (SM), which acts as the back reflector. The RM is located at a distance of 1630 mm from the 400 mm lens, while the back reflector with a radius of curvature of 4000 mm is positioned at a distance of 4830 mm from the RM. Distances were measured with a tape measure. In order to reduce the overall size of the setup, the 4830 mm path was folded by the insertion of a flat mirror (FM) (not shown) between RM, and SM, FM. We should also note that since the SM is not involved in the imaging, it can be replaced by a FM.

For monitoring the rotation, we also placed a standard silicon photodiode (Thorlabls PD136A) close to the RM: when rotating, the mirror diverts the laser light to the diode eight times per revolution, thereby, producing a well-defined potential spike that can conveniently be recorded on an oscilloscope.

The light reflected by the SM travels along the same path, except that it is diverted to a webcam (Logitech C310) by a pellicle beam splitter (BS, Thorlabs BP150) positioned to the left of FP, which is the focal point of L_1. The small lens of the webcam has to be removed before use, so that no extra imaging element is introduced. In the original version of the experiment, instead of a camera, a microscope is used to measure the displacement of the beam. However, given the finite size of the focal spot, this also entails that large distances have to be employed in order to realize measurable displacements. The application of the camera not only makes data collection more convenient, but it also implies that the physical size of the setup can be considerably reduced. We would like to point out that the use of a webcam in the context of speed of light measurements was discussed in an interferometric setting in [7].

Our second setup, setup 2, is shown in figure 3. The light of the fault locator is focused by a lens of focal length 400 mm onto FP, from where it reaches the SM with a focal length of

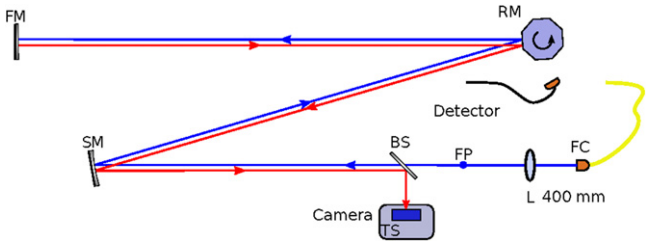

Figure 3. Experimental setup, setup 2. RM, FM, and SM are the rotating, flat, and spherical mirrors, respectively, L is a lens of focal length 400 mm, FC is the fibre collimator, BS is the beamsplitter, and TS are translation stages. Dimensions as indicated in the text.

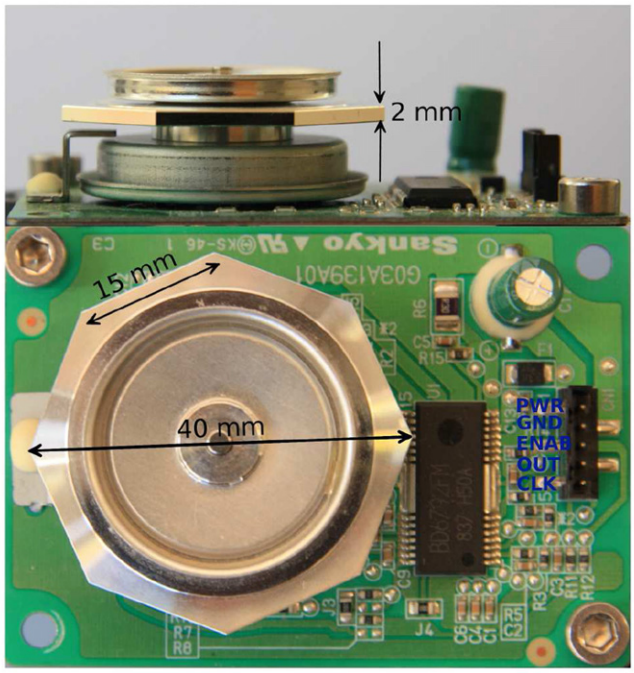

Figure 4. Rotating printer mirror, side view (top), and top view (bottom). The 30-pin integrated circuit contains the motor driver (BD6792FM from Rohm Semiconductors) with the built-in PLL. Control pins are labelled in blue and are explained in the text.

2 m. The SM is 4060 mm away from FP, and is tilted slightly, so that the light is reflected off the RM, located 730 mm away from SM, and finally FM, located 3260 mm away from RM. The lengths in the setup are chosen in such a way that the light is focused on the flat end reflector, FM, although, as will be discussed in section 6, small longitudinal misalignments do not influence the results in any significant way. As in the first setup, folding mirrors were used between SM, and RM, and between RM, and FM.

The two setups are conceptually the same: the only difference between them is that the imaging element in the first case is a lens, while in the other case, it is a SM.

As the rotating reflector, we employed an octagonal printer mirror scavenged from a faulty printer, shown in figure 4. (This part can also be purchased separately. A possible alternative is a barcode reader with a revolving mirror.) Laser printers utilize a focused laser beam to locally discharge a positively pre-charged cylindrical drum, that is itself rotating around its own axis. The octagonal (sometimes quadratic, or hexagonal) mirror is used for scanning the laser beam along the axis of the drum, thereby creating an accurate time-to-two-dimensional mapping on the drum's surface. In order to achieve high spatial accuracy, both the drum and the RM have to revolve at a constant speed. Stabilization of the rotation frequency is achieved by means of phase-locked loops (PLL), in which an external clock signal is locked to the signal of a magnetic field transducer measuring the temporal variations of the field of a constant magnet moving with the axle of the motor. This also means that, within limits, the rotation speed can be set by adjusting the clock signal that is fed into the PLL loop. Figure 4 also indicates the connections of the mirror assembly: PWR (pin 1) is the power line, whose potential can be anything between +18, and +36 V, GND (pin 2) is ground, ENAB (pin 3) is the active-low motor enable pin (this should be tied to ground), while CLK (pin 5) is the clock line, which takes TTL pulses with frequencies between around 300, and 6000 Hz. Pin 4 is an output connected to the magnetic field transducer, and can be used for monitoring the rotation.

The advantages of the mirror assembly are that first, the mirror is monolithic, therefore, it is safe to operate: no pieces can break off at high speeds. Second, the control electronics makes it possible to adjust the speed by setting the frequency of the clock signal from a simple function generator, and that there is a well-defined linear relationship between the rotation speed and the clock frequency.

Initial alignment of the setup is performed when the mirror is stopped (the enable line is high). First, all mirrors are placed at their respective positions, and FC is aligned such that the collimated laser beam can travel to the end mirror, SM. Then L_1 is inserted in such a way that the diverging laser light still reaches both RM, and SM. After this, L_2 is inserted in the path, and is moved along the optical axis till the size of the light spot reaches its minimum on SM. When this is achieved, the beamsplitter, BS, has to be placed on the left-hand side of the focal point of L_1, at a distance of about 5–7 cm from the focal spot, FP. With the tip-tilt control knobs of the mirror holder, SM has now to be aligned so that the light is reflected back to the laser. At this point, the reflected beam should be focused on FP. Finally, the camera has to be placed in the diverted focus of the back-reflected beam. Great care has to be taken to make sure that the camera's plane is as perpendicular to the laser beam as possible: failure to do so will results in a systematic error, which leads to higher speeds of light. For a thorough discussion on this, see section 6.

5. Experimental results

As can be inferred from equation (2), in order to determine the speed of light, one has to measure $d_{1,2,3}$, the angular frequency ω, and the displacement Δs. The measurement can be done in the same way in both setups, and the steps are as follows. First, one has to determine the rotation speed as a function of the clock frequency. Next, the pixel size of the camera has to be measured. This step amounts to calibrating a ruler. Then the displacement of the image on the camera has to be measured at various clock frequencies (this step involves fitting to the camera images), and by using the pixel size, this displacement has to be converted to physical units. Finally, the slope of the displacement–frequency relationship has to be determined, and inserted in equation (2).

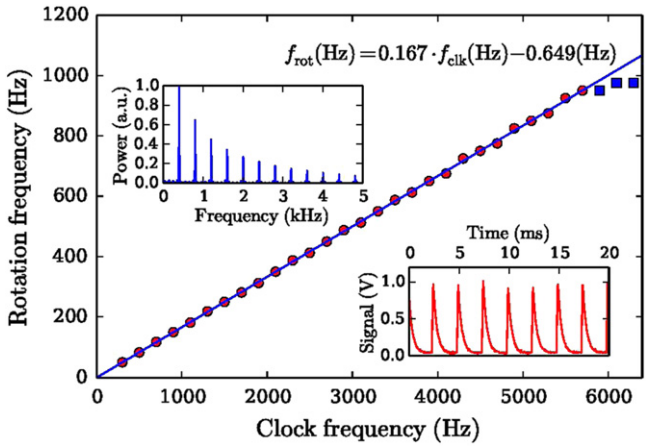

Figure 5. Rotation speed as a function of clock frequency. The inset in the lower right corner shows a typical time trace on the detector with its Fourier spectrum in the upper left. The clock frequency for this trace is 300 Hz. The parameters of a linear fit are displayed in the figure. The last three data points (blue squares) were excluded. The error in the slope is 0.000 54.

The rotation speed can be deduced from the time traces of the photodiode, either by simply measuring the time difference between an integer number of maxima, or recording the potential values, taking the Fourier transform, and identifying the strongest frequency component. Given a high enough number of samples, the two methods deliver the same results. In figure 5, we show the measured rotation speed as a function of the clock frequency, with a typical time trace of the detector signal on an oscilloscope, and its Fourier transform. The period can clearly be resolved from either the signal, or its Fourier spectrum. Note that at high clock rates, the rotation speed saturates. For this reason, we excluded the last three points from the linear fit, from which we deduced the relationship $f_{\mathrm{rot}}\,(\mathrm{Hz}) = (0.167 \pm 0.000\,54) \cdot f_{\mathrm{clk}}\,(\mathrm{Hz}) - 0.649\,(\mathrm{Hz})$. The error of the fit is approximately 0.3%. Given the precision (in the ppm range) of frequency standards used in modern pulse generators, and the stability of PLL used in laser printers, we ascribe the error to our way of determining the frequency from the Fourier transform of the time trace. Also note that, since the RM has eight facets, the actual rotation speed is only 1/8 of what the detector signal indicates.

It is worth pointing out that, given the order of magnitude of the rotation speed, in the absence of an oscilloscope, these frequencies can easily be measured by means of a smart phone. All one has to do is to convert the electrical signal of the photodiode to sound by amplifying it, and connecting it to a speaker, and then record the sound through the microphone. There are countless applications that can take and display the Fourier transform of the microphone input. Likewise, the clock signal can be generated by a suitable waveform applied to the phone's speaker.

In order to convert the pixel positions into physical distance, we have to calibrate the CCD camera. In other words, we have to measure the pixel size. For this procedure, we stopped the RM, and shifted the camera by an amount indicated by the micrometre screw on the translation stage. The data points are plotted in figure 6 in conjunction with a linear fit, which gives a pixel size of 2.75 μm. This is also the value given by the manufacturer. By the help of this measurement, one can also ascertain that the translation axis is parallel to the

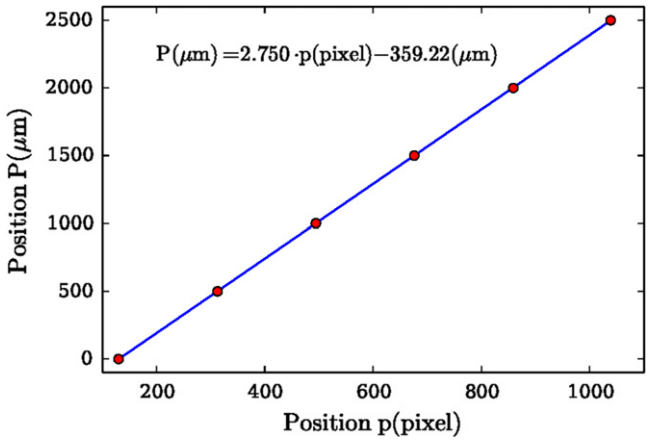

Figure 6. Measurement of the pixel size. The statistical errors in both the dependent and independent variables are too small to be visible. The parameters of the linear fit are indicated in the figure.

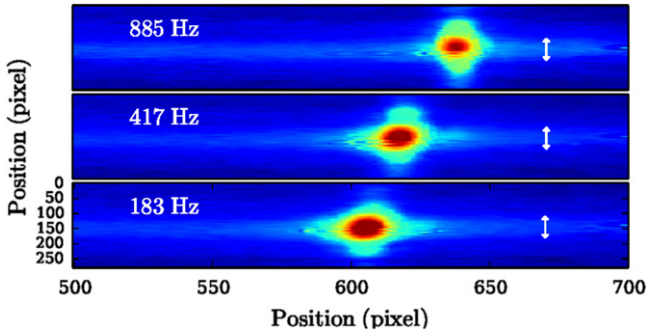

Figure 7. Typical camera images in setup 1 at rotation frequencies 183, 417, and 885 Hz, respectively. The profiles below were obtained by integrating over the region indicated on the right-hand side by the small white arrows.

camera's plane, because if that is not the case, then the width of the profiles changes as the camera is shifted. As shown below (see, e.g., figure 8), the centre of the nearly Gaussian profiles can be obtained with sub-pixel accuracy. If we take half of the smallest micrometre division (10 μm) as the error in position, this procedure incurs an overall error of less than one fifth of a per cent.

Having determined the calibration for both the cameras, and the rotation speeds, we now turn to the measurement of the displacements. First we discuss the results obtained from setup 1. Typical images of the reflected beam at three different rotation speeds (183, 417, and 885 Hz) are shown in figure 7 (only a small part of the otherwise 720-by-1280 chip is displayed). The movement of the beam is clearly visible. Note that, while we begin with a circularly symmetric Gaussian beam (this is what leaves the single-mode fibre), the camera image is elongated along the vertical direction, which is perpendicular to the direction of the displacement. The reason for this is that the RM is only 2 mm thick, but 15 mm wide, while the beam at the mirror's position is still about 10 mm in diameter. This means that diffraction will stretch the beam in the direction of the smallest dimension of the mirror.

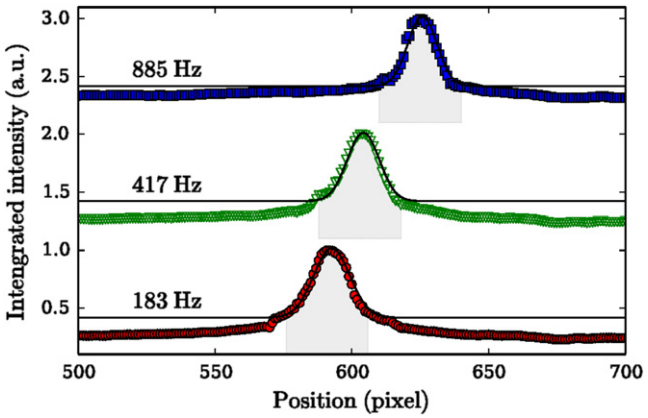

Figure 8. Typical profiles taken in Setup 1 at a rotation frequency of 183 (solid red circle), 417 (empty green triangle), and 885 Hz (solid blue square), respectively. The domain of Gaussian fits is indicated by the shaded grey regions, while the solid black lines are the fits.

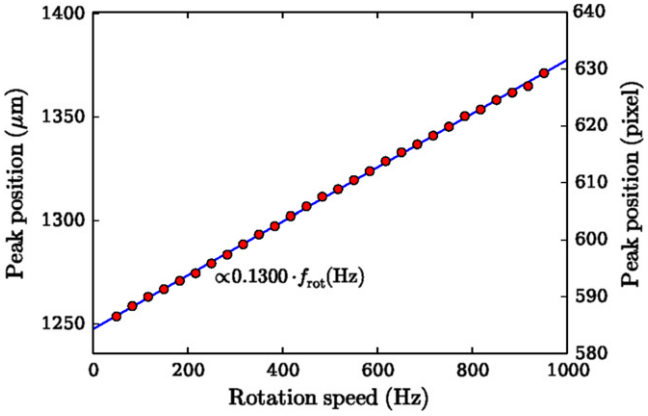

Figure 9. Position of the reflected beam as a function of the rotation speed in setup 1. On the right vertical axis, the same data are shown in units of the CCD pixels. The peak position can be obtained from $P_{\text{peak}}\,(\mu\text{m}) = (0.130 \pm 0.00047) \cdot f_{\text{rot}}\,(\text{Hz}) + 1247.6\,(\mu\text{m})$. Statistical error bars on the data points are not visible.

The images in figure 7 are turned into nearly Gaussian profiles by vertically integrating over a range of ±25 pixels around the maximum, as indicated by the small white arrows in the figure. Such profiles for three different rotation speeds (183, 417, and 885 Hz) are shown in figure 8. In order to accurately determine the centre positions of these profiles, we fit a Gaussian with an offset to the data points in a range of ±15 pixels around the pixel with the highest intensity, as shown by the shaded grey domains in the figure. The centre of these fits is then accepted as the true position of the reflected beam. The error in the fit is less than 0.15 pixels for all measurements.

Figure 9 contains measurement data on the beam displacement as a function of the rotation speed. On the right vertical axis, the positions are given in terms of the CCD pixels, as taken from images similar to figure 7. The left axis displays the positions in physical units,

after the CCD pixels were converted using the fit from figure 6. The linear fit to these data yields a slope of $(0.130 \pm 0.000\,47)\ \mu\text{m Hz}^{-1}$. Given that, with the nomenclature of equation (2), $d_1 = 425 \pm 1$ mm, $d_2 = 1630 \pm 1$ mm, and $d_3 = 4830 \pm 1$ mm, and taking all above-mentioned error sources into account, we calculate a speed of light of $c = (2.97 \pm 0.03) \times 10^8\ \text{m s}^{-1}$. This is within 1% of the defined value of $2.997\,924\,58 \times 10^8\ \text{m s}^{-1}$, and overall, the statistical errors are within 1%.

We now discuss measurements in setup 2. Typical camera images at frequencies 50, 400, and 751 Hz, respectively are shown in figure 10. As opposed to the other setup, the laser spot is stretched vertically over the whole length of the camera (720 pixels). Also note that as the frequency increases, so does the width of the images. We speculate that this might be related to turbulence generated by the fast RM: while the average speed of the motor is determined by the clock frequency, vortices detaching from the vertices of the octagonal mirror can lead to fluctuations in the instantaneous speed.

This change in the width can also be seen in figure 11, where we plot the vertically integrated camera images for 17 rotation frequencies as indicated. However, despite the broadening of the profiles, the displacement is clearly visible as the frequency changes.

In figure 12 we plot the beam displacement as a function of the rotation speed, similar to figure 9. The linear fit to these data yields a slope of $(0.899 \pm 0.0059)\ \mu\text{m Hz}^{-1}$. Given that $d_1 = 4060 \pm 1$ mm, $d_2 = 730 \pm 1$ mm, and $d_3 = 3260 \pm 1$ mm, and considering all error sources, we calculate a speed of light of $c = (3.02 \pm 0.03) \cdot 10^8\ \text{m s}^{-1}$.

Our experimental conditions and results are summarized in table 1.

6. Systematic errors

We have already indicated the magnitude of statistical errors: the calibration of the CCD is about 0.2%, the rotation frequency's is about 0.3%, the length measurement's is less than 0.1%, while the Gaussian fits to the profiles contain an error of about 0.2%. However, in addition to these, there are a number of systematical errors that one has to consider.

One we have already pointed out, namely, if the camera is not perpendicular to the laser beam, all displacements will be measured *shorter* and this will lead to a seemingly *larger* speed of light. One way of removing this error source is to slightly rotate the camera without moving it, and repeat the measurements multiple times. The smallest value of c should correspond to the perpendicular configuration. However, since this correction is proportional to the cosine of the angle of deviation from the normal, errors are of second order.

Second, if the camera's plane is not parallel to the axis of the translation stage, the pixel size will be inferred incorrectly, and this, again, will lead to a seemingly higher light speed. As mentioned above, a trivial test for this is the beam profile measured at various positions of the translation stage: all other conditions being identical, a simple translation should result in identical profiles. If this is not the case, then the camera has to be rotated slightly with respect to the translation stage till all measured profiles are identical. As with the systematic error discussed above, corrections are quadratic in the angle.

Third, the measurement of independent quantities, in this case, the frequency (time) and distance might contain errors that result from the particular method used to measure them. Given the accuracy of frequency measurements, it is reasonable to expect that only the value of distance would be affected, and one can safely neglect systematic errors in frequency.

Fourth, imperfections in the focusing lead to small errors. In order to estimate the order of magnitude of these, let us assume that the image of S is formed not at the end mirror, but at P, which is at a distance of x from M, as shown in figure 13. The virtual image of P will also be

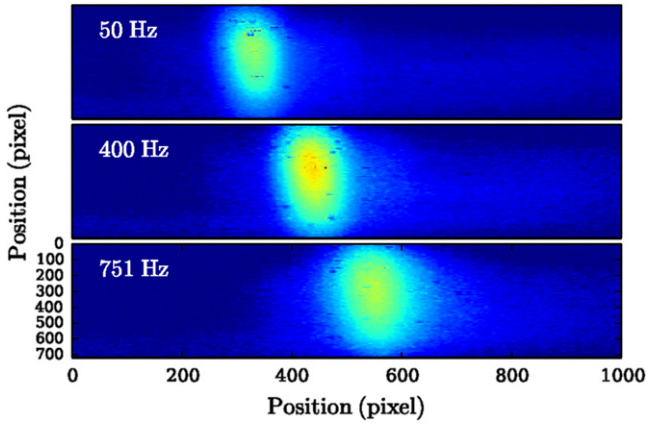

Figure 10. Camera images in setup 2 at frequencies 50, 400, and 751 Hz.

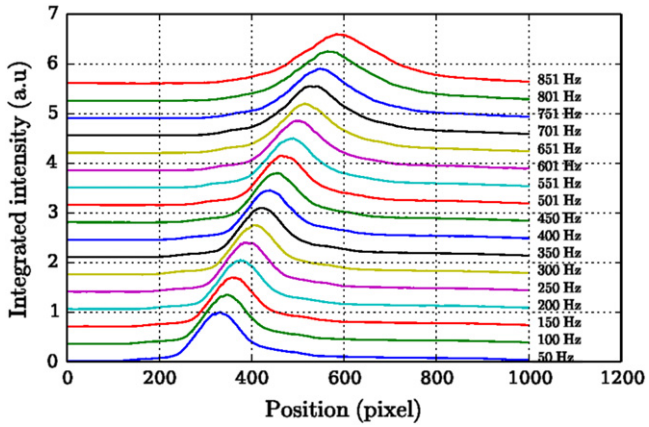

Figure 11. Vertically integrated camera profiles in setup 2 as a function of the frequency.

shifted by the same amount, and following the derivation in section 3, we arrive at

$$c = \frac{4d_1d_3(d_3 - x)}{d_2 + d_3 - x}\left(\frac{\mathrm{d}\Delta s}{\mathrm{d}\omega}\right)^{-1} \approx c_0\left[1 - \frac{xd_2}{d_3(d_2 + d_3)}\right], \tag{3}$$

if $x \ll d_3$. Note that d_1 does not necessarily indicate the distance at which the image is formed: it simply designates the position of the measurement (webcam). If d_1 is chosen such that the imaging condition is not satisfied, it does not mean that the derivation is incorrect, it only means that the image will not be sharp at that point, but equation (3) is still valid.

The magnitude of the correction will depend on two parameters of the setup, d_2, d_3, and the inaccuracy in the focusing, x. Note that for $d_2 = 0$, i.e., when the RM is next to the imaging element, the first-oder correction is zero. In the first setup $d_2/d_3 \approx 1/3$, while in the second case, $d_2/d_3 \approx 1/4$. Therefore, an upper bound for the correction in equation (3) is $x/(4d_3)$. Given that $d_3 \geqslant 3$ m, we incur an error of 1%, if $x \approx 0.12$ m. It is reasonable to assume that the focus can be determined with 10 cm accuracy, even if the imaging elements

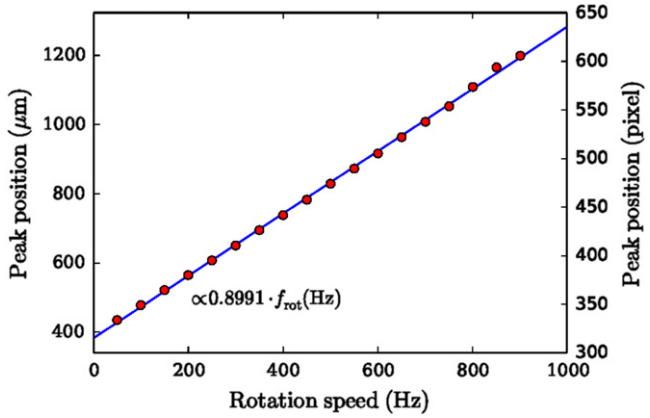

Figure 12. Position of the reflected beam as a function of the rotation speed in setup 2. On the right vertical axis, the same data are shown in units of the CCD pixels. The linear fit to the peak position is $P_{\text{peak}}\,(\mu\text{m}) = (0.899 \pm 0.0059) \cdot f_{\text{rot}}\,(\text{Hz}) + 383.3\,(\mu\text{m})$. Error on the data points is not visible.

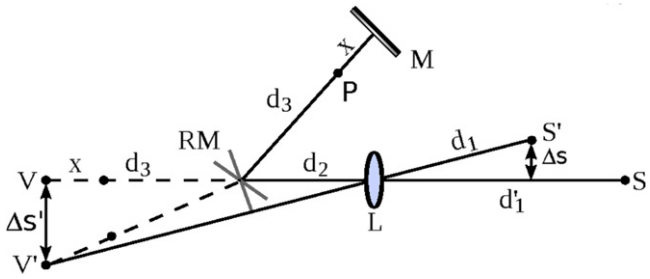

Figure 13. The concept of the measurements, with focusing errors. Notation as in figure 1. *P* is the image of the source *S*.

Table 1. Summary of experimental conditions, and results. Overlines denote distances between designated elements.

	d_1	d_2	d_3	c (m s^{-1})
Setup 1	$\overline{\text{FP} - L_2}$	$\overline{L_2 - \text{RM}}$	$\overline{\text{RM} - \text{SM}}$	2.97×10^8
	425 mm	1630 mm	4830 mm	
Setup 2	$\overline{\text{FP} - \text{SM}}$	$\overline{\text{SM} - \text{RM}}$	$\overline{\text{RM} - \text{FM}}$	3.02×10^8
	4060 mm	730 mm	3260 mm	

have such long focal length. Therefore, we can conclude that the error related to imperfect focusing is less than 1%.

Finally, the lens, the only glass element in the first setup, has finite width with a refractive index larger than one, and this adds to the total length between the focal point and the end mirror. This extra optical length can be measured and added to the path, provided the

refractive index of the glass is known. Of course, the second setup does not suffer from this kind of error.

7. Conclusion

In conclusion, we presented a simple version of the Foucault method for the measurement of the speed of light. We demonstrated that with readily available and inexpensive optics, and a bit of data processing, acceptable accuracy (results within 1% of the defined value) can be achieved. We also discussed a range of systematic errors, and pointed out several possible improvements. The experiment teaches students the historically important Foucault method, and modern data evaluation concepts at the same time.

Appendix. MATLAB code

Here we list matlab snippets that can be used for the evaluation of images. The usual workflow is to create a profile similar to that in figure 8 with the function `create_profile`, and pass the output to the function `fit_profile`, which will print the parameters of the best Gaussian fit to the console. `gauss` simply defines the fit function, and it can easily be replaced by other, more appropriate forms, if necessary.

```
function profile = create_profile(fn, range1, range2)
    % Returns and displays a profile (a vertically integrated image segment)
    %
    % Input:
    %
    % fn: the file (camera image) to read
    % range1, range2: the limits of the vertical intagration
    im = imread(fn);
    im1=sum(im, 3); % Turns the RGB image int ograyscale
    figure(1); imagesc(im1)
    profile = sum(im1(range1:range2,:));
    figure(2); plot(profile, 'ro');
```

```
function y=gauss(par, xdata)
            % Returns a Gaussian function evaluated at points given in xdata
            %
            % y = A* exp(-(x-x0)^2/sigma^2)+offset
            %
            % Input:
            % par: an array of parameters in the form[ A, x0, sigma, offset]
            % A: amplitude of the Gaussian
            % x0: centre of the Gaussian
            % sigma: standard deviation of the Gaussian
            % offset: offset of the Gaussian
            % xdata: points where the function is to be evaluated
            y=par(1) * exp(-(xdata-par(2)).^2/par(3)/par(3)) + par(4);
```

```
function fit_profile(profile, xlim1, xlim2, par)
```

(Continued.)

```
% Fits a profile with a Gaussian
%
% Input:
% profile: a 1D array of evenly spaced measurement points
% xlim1, xlim2: the fit will be done on domain[ xlim1:xlim2]
% par : initial guess of the fit (see gauss(par, xdata))
f=lsqcurvefit(@gauss, par, xlim1:xlim2, profile(xlim1:xlim2))
figure(3); hold on; plot(xlim1:xlim2, profile(xlim1:
  xlim2),'ro')
plot(xlim1:xlim2, gauss(f, xlim1:xlim2),'b-');
hold off;
```

References

[1] 17th Conférence Générale des Poids et Mesures (CGPM) 1984 http://bipm.org/en/CGPM/db/17/1/
[2] Measurement According To Foucault/Michelson 2012 http://ld-didactic.de/literatur/hb/e/p5/p5611_e.pdf
[3] Speed of Light Experiment 2012 http://pasco.com/prodCatalog/EX/EX-9932_speed-of-light-experiment/.
[4] Clark G W 1956 *Am. J. Phys.* **24** 189
[5] Clark G W 2001 *Am. J. Phys.* **69** 110
[6] Belich T J, Lahm R P, Peterson R W and Whipple C D 1996 *Am. J. Phys.* **65** 186
[7] Lahaye T, Labastie P and Mathevet R 2012 *Am. J. Phys.* **80** 497
[8] DOrazio D J, Pearson M J, Schultz J T, Sidor D, Best M W, Goodfellow K M, Scholten R E and White J D 2010 *Am. J. Phys.* **78** 524
[9] Dillman L T 1964 *Am. J. Phys.* **32** 567
[10] Feagin J M 1979 *Am. J. Phys.* **47** 288
[11] Morrison H M and Driedger J A 1980 *Phys. Educ.* **15** 100
[12] Brody J, Griffin L and Segre P 2010 *Am. J. Phys.* **78** 650
[13] Rogers J, McMillan R, Pickett R and Anderson R 1969 *Am. J. Phys.* **37** 816
[14] Deblaquiere J A, Harvey K C and Hemann A K 1991 *Am. J. Phys.* **59** 443
[15] Aoki K and Mitsui T 2008 *Am. J. Phys.* **76** 812
[16] Ronzani A, Maccarrone F and Lieto A D 2008 *Eur. J. Phys.* **29** 957
[17] Bates H E 1988 *Am. J. Phys.* **56** 682